The origin of multiple spin-relaxation channels below the metal–insulator transition in ferromagnetic colossal magnetoresistance (CMR) manganites

2004 J. Phys.: Condens. Matter 16 S4541

(http://iopscience.iop.org/0953-8984/16/40/008)

INSTITUTE OF PHYSICS PUBLISHING JOURNAL OF PHYSICS: CONDENSED MATTER

J. Phys.: Condens. Matter **16** (2004) S4541–S4562 PII: S0953-8984(04)84323-6

The origin of multiple spin-relaxation channels below the metal–insulator transition in ferromagnetic colossal magnetoresistance (CMR) manganites

R H Heffner[1], D E MacLaughlin[2], G J Nieuwenhuys[3] and J E Sonier[4]

[1] Los Alamos National Laboratory, MS K764, Los Alamos, NM 87545, USA
[2] Department of Physics, University of California, Riverside, CA 92521, USA
[3] Kamerlingh Onnes Laboratory, Leiden University, PO Box 9504, 2300 RA Leiden, The Netherlands
[4] Department of Physics, Simon Fraser University, Burnaby, BC V5A 1S6, Canada

Received 8 April 2004
Published 24 September 2004
Online at stacks.iop.org/JPhysCM/16/S4541
doi:10.1088/0953-8984/16/40/008

Abstract

We report a series of measurements in (La, Ca, Pr)MnO_3 compounds which show that ferromagnetic (FM) CMR compounds develop two Mn-ion spin–lattice relaxation channels as the materials are cooled below their insulator-to-metal transition temperature T_{MI}. This result is in contrast to conventional FMs and is attributed to the presence of both insulating and conducting FM regions below T_{MI} which coexist on a microscopic scale. The coexistence of different phases is found in both polycrystalline and single-crystalline materials, though the single crystal exhibits a narrower temperature region of phase coexistence below its FM critical temperature T_C. Possible differences between crystalline and granular materials which could give rise to these findings are discussed. These results could have important implications for the use of CMR materials in spintronics devices, which rely on conducting surfaces in thin film multilayers below T_C.

1. Introduction

The study of perovskite-structured Mn-based materials possessing coupled spin–charge–lattice degrees of freedom has been underway for decades [1]. The earliest investigations involved the substitution of divalent alkaline earth elements such as Ca, Ba or Sr into $LaMnO_3$, an insulating antiferromagnet (AFM). For sufficient concentrations of the alkaline earths this results both in a metal–insulator (MI) transition and a ferromagnetic ground state via the double-exchange interaction [2]. This was already understood in the 1950s [3]. Renewed interest in these materials was triggered in the 1990s by the discovery that a 'colossal' reduction ($\times 10$) in resistance occurs near the metal–insulator transition temperature T_{MI} by the application of relatively modest (a few tesla) applied magnetic fields [4]. This discovery has generated a

huge amount of work over the last decade, resulting in the discovery of new phenomena and stimulating additional theoretical activity. In particular, it is now known that in order to explain the magnitude of the 'colossal magnetoresistance' (CMR) in these materials one must include the effects of lattice distortions [5, 6] which occur as a result of the Jahn–Teller interaction in the excited e_g d-spin Mn^{3+} orbitals. In addition, it has been established that the Mn orbitals tend to order [7], and that this orbital ordering correlates with the magnetic spin structure. These materials are also known to exhibit ordered sublattices of charge called charge ordering (CO) [8]. Because the charge transport deep in the FM state is highly spin polarized [9], CMR materials are also under intense investigation for their possible use in spintronics devices [10]. Thus, the field of CMR physics has flourished because of the excitement generated by the underlying physics and the potential utility for device applications.

In this paper we report on muon spin relaxation (μSR) experiments in selected perovskite manganites, primarily in the $La_{1-x}Ca_xMnO_3$ series of compounds. Our primary focus is the documentation and explanation of the observation of two distinct Mn relaxation channels in ferromagnetic (FM) CMR materials. Why is this important? First, conventional homogeneous FMs exhibit only a single relaxation channel above and below the Curie temperature T_C. Both neutron scattering [11] and μSR [12] experiments demonstrate conclusively that in the low-doping region of the $La_{1-x}Ca_xMnO_3$ phase diagram magnetic inhomogeneities exist. However, the prevailing wisdom regarding $La_{1-x}Ca_xMnO_3$ ferromagnets near optimal doping ($x = 3/8$, where T_C is maximized) has been that the system reaches a homogeneous state just a few degrees below T_C due to the long-range transport of the doped holes that give rise to a metallic state [6]. Thus, our initial observation of multiple (>1) relaxation channels significantly below T_C was puzzling [13].

A second reason why the discovery of more than one relaxation channel in CMR ferromagnets is important is our conclusion that this effect arises from coexisting conducting and insulating FM regions below the metal–insulator transition. We demonstrate that two relaxation modes are found both in polycrystalline samples and in a single crystal which has been well studied and, hence, 'vetted' by other techniques. This coexistence of insulating and conducting regions could have important implications for the application of CMR materials in magnetoresistive devices, such as magnetic tunnel junctions, where even a thin layer of insulating surface material can degrade performance.

Many of the early data from our group have already been published in several different articles. The purpose of this paper is to bring together in one place selected data sets that provide a direct and easy comparison between previously published results. Other previously published data that are not essential to understanding the basic theme of two relaxation channels will only be summarized here. The Knight shift data in $La_{0.35}Pr_{0.35}Ca_{0.30}MnO_3$ and the data on single-crystal $La_{0.75}Ca_{0.25}MnO_3$ are new. We point out that, in addition to the experiments reported here, other μSR work in the $La_{1-x}Ca_xMnO_3$ series finds inhomogeneous spin–lattice relaxation as well [14].

This paper is organized as follows. Section 2 contains the general physics concepts underlying CMR materials. In section 3 we briefly describe the details of the μSR technique relevant to the experiments reported here. The experimental results are presented in section 4, and section 5 contains the discussion and the conclusions.

2. CMR materials

The structure of $LaMnO_3$ is orthorhombic with room-temperature axes $a = 5.542$ Å, $b = 5.732$ Å and $c = 7.683$ Å. The Mn atoms reside at (0, 0.5, 0), oxygen O(1) at (0.073, 0.485, 0.25) and oxygen O(2) at (0.224, 0.304, 0.039), in units of the lattice constants. The

ground-state electronic structure [6] of Mn^{3+} in $LaMnO_3$ consists of five electrons residing in three degenerate t_{2g} d-wave orbitals and two excited e_g d-wave orbitals elevated in energy by the crystalline electric fields. The latter are themselves split by the Jahn–Teller (JT) interaction when occupied. A strong Hund's rule coupling aligns the spins in the ground and excited states. Magnetic order is produced through the super-exchange interaction occurring between neighbouring Mn atoms. The Goodenough–Kanamori rules [3] and the ordering of the Mn e_g orbitals account for the nearest neighbour FM interactions in the plane and the antiferromagnetic (AFM) ordering between planes. When doped with Ca^{2+}, for example, $La_{1-x}Ca_xMnO_3$ develops x Mn^{4+} atoms due to the introduction of x holes. Charge transport occurs solely by the movement of these holes between Mn e_g states through the neighbouring oxygen p orbitals. Long-range transport of this nature is obviously forbidden without electron or hole doping, and thus both $CaMnO_3$ and $LaMnO_3$ are insulators. A hole in (La, Ca) MnO_3 hops from a Mn^{4+} site to a neighbouring Mn^{3+} site, and thus the JT distortion must be 'dragged' from one Mn site to the next, costing energy. Furthermore, the very strong on-site Hund's rule coupling guarantees that the transported e_g spins must be aligned with the core t_{2g} spins at the new site, leading to FM via the double-exchange interaction. Ferromagnetic alignment only happens at sufficiently high doping that the energy gained by hole delocalization outweighs the energy cost of overturning the neighbouring antiferromagnetically aligned spin and dragging along the lattice distortion. Above the Curie temperature, the slowly hopping hole, together with its JT distortion, is often called a magnetoelastic polaron.

The $La_{1-x}Ca_xMnO_3$ series of materials remains orthorhombic below about 700 K from $x = 0$ to 1 [15]. In addition to the insulating AFM end members, $LaMnO_3$ and $CaMnO_3$, and the onset of FM with low Ca doping, one finds regions of the phase diagram which exhibit CO (and thus insulating behaviour), where the Mn^{3+} and Mn^{4+} sit on ordered sublattices. In general, the degree of conducting or insulating behaviour depends upon the cation size mismatch between the La atom and the alkaline earth atom [16]. Among the alkaline earth atoms Sr, Ca and Ba, Sr produces the least distortion and Ba the most.

3. μSR technique and other experimental details

3.1. Fitting the data

The μSR technique [17] employed here involves the interstitial implantation of positive muons with essentially 100% spin polarization, oriented antiparallel to the initial muon momentum vector. The muon decays with a mean lifetime τ_μ of 2.2 μs into a positron and two undetected neutrinos. The positron is emitted preferentially along the muon spin direction. Detection of the positron emission rate as a function of angle relative to the initial muon spin direction allows one to monitor the time rate of decay of the muon spin polarization, and, hence, the magnitude and time-correlation of the internal magnetic fields in the sample.

Three basic types of experiments are described here. Zero-field (ZF) experiments are carried out with no applied field, while longitudinal-field (LF) experiments are performed with an applied field along the initial muon spin direction $\vec{S}(0)$, taken to be the z-axis. The positron emission rate $\mathrm{d}N/\mathrm{d}t$ in ZF or LF is given by

$$\mathrm{d}N/\mathrm{d}t = B + N_0(1/\tau_\mu)\exp(-t/\tau_\mu)[1 \pm AG(t)] \tag{1}$$

where N_0 is a normalization factor, B is a time-independent background and A is the average asymmetry of the decay angular distribution (typically 0.2–0.3). The + and − signs correspond to positron detection angles of 0° and 180° relative to $\vec{S}(0)$, respectively. The function $G(t)$ describes the time rate of decay of the muon spin polarization. We label $G(t) = G_z(t)$ in ZF

and LF experiments, where $G_z(t)$ gives the spin–lattice relaxation rate(s) from the electronic spins, whose coupling to the muon occurs through dipole and transferred hyperfine fields, which usually dominate the fields from the ever-present nuclear spins.

The μSR data presented here were taken at the M20 muon channel at TRIUMF (Vancouver, Canada) and on the GPS spectrometer at the Paul Scherrer Institute (Villigen, Switzerland). The ZF data could be fitted to a relaxation function

$$G_z(t) = A_{\rm O} G_{\rm osc}(t) + A_{\rm R} G_{\rm rlx}(t), \tag{2}$$

corresponding to oscillating and relaxing terms, respectively. In zero applied field the oscillating component $G_{\rm osc}(t)$ occurs in a magnetically ordered state, and is given by

$$G_{\rm osc}(t) = \sum_i (A_{\rm osc})_i \exp(-t/T_{2i}) \cos(2\pi \nu_i t + \varphi_i) \tag{3}$$

where $(A_{\rm osc})_i$ is the amplitude of the ith precessing component, ϕ_i is a phase angle and ν_i and $1/T_{2i}$ are the corresponding muon precession frequency and inhomogeneous damping rate. We define $\sum_i (A_{\rm osc})_i \equiv 1$. The existence of multiple frequencies can be due to more than one muon lattice site and/or different microscopic magnetic environments (even for a single muon lattice site).

In our ZF experiments the relaxing component $G_{\rm rlx}(t)$ frequently approximates a stretched-exponential form:

$$G_{\rm rlx}(t) = \exp[-(t/T_1)^K], \tag{4}$$

where $1/T_1$ is a characteristic spin–lattice relaxation rate. The polycrystalline averages of $A_{\rm R}$ and $A_{\rm O}$ in a magnetically ordered state (where both $A_{\rm R}$ and $A_{\rm O}$ are non-zero) are $A_{\rm R} = 1/3$ and $A_{\rm O} = 2/3$. For rapid fluctuations the muon relaxation rate $1/T_1$ is given by

$$1/T_1 \propto \gamma_\mu^2 \sum_q |\delta B(q)|^2 \tau(q), \tag{5}$$

where $|\delta B(q)|$ is the amplitude of the fluctuating local field and $\tau(q)$ is the Mn-ion correlation time. The sum over the characteristic momenta q of the Mn-ion excitations occurs because the muon is a local probe. When the exponent in equation (4) $K < 1$ a distribution of $1/T_1$ values is implied [18], and thus $|\delta B(q)|$ and/or $\tau(q)$ are distributed. Typically, near a magnetic phase transition the correlation time becomes longer, causing $1/T_1$ to increase, a phenomenon known as critical slowing down. Below the ordering temperature, the fluctuating amplitude decreases and $1/T_1$ is reduced.

The stretched exponential form in equation (4) is often useful to parametrize the data because it involves only a few parameters and can be used to approximate $G_{\rm rlx}(t)$ over a wide temperature range. However, for the materials under investigation here, we have found that for large $1/T_1$ and small K the relaxation function can often be better approximated over a limited temperature range by the sum of two exponentials:

$$G_{\rm rlx}(t) = A_{\rm f} \exp(-\lambda_{\rm f} t) + A_{\rm s} \exp(-\lambda_{\rm s} t), \tag{6}$$

where $\lambda_{\rm f}$ and $\lambda_{\rm s}$ correspond to fast and slow local-field fluctuation rates τ^{-1}, respectively. We define $A_{\rm f} + A_{\rm s} = 1$. This fitting function is for a bimodal distribution of fluctuation rates, and its appropriateness is discussed in detail in section 4.3 below.

In a TF μSR experiment an external field is applied perpendicular to $\vec{S}(0)$. In general, for TF fields,

$$\mathrm{d}N/\mathrm{d}t = B + N_0(1/\tau_\mu) \exp(-t/\tau_\mu) \left[1 + \sum_i A_i G_{xi}(t) \cos(2\pi \nu_i t + \phi_i) \right], \tag{7}$$

where ϕ_i is a fixed phase angle corresponding to the positron detection angle. The subscripts i refer to multiple precessing components, as described above for ZF experiments. The relaxation function $G(t) = G_x(t)$ describes the spread in local fields, e.g., for a Lorentzian field distribution $G_x(t) = \exp(-t/T_2)$. The magnitude of the local field $|\vec{B}|$ (applied field plus internal fields) is given by $\omega_i = 2\pi\nu_i = \gamma_\mu|\vec{B}|$, where the muon's gyromagnetic ratio $\gamma_\mu = 8.51 \times 10^8$ Hz T^{-1}.

3.2. Sample preparation

The $La_{1-x}Ca_xMnO_3$ and $La_{0.35}Pr_{0.35}Ca_{0.30}MnO_3$ samples studied here were polycrystalline materials prepared either as boules in an optical floating zone furnace ($0 \leqslant x \leqslant 0.18$) or as [15, 16] sintered powders ($0.33 \leqslant x \leqslant 1.0$) using a conventional solid state reaction in air. In general, polycrystalline materials of (La, Ca)MnO_3 can be more compositionally homogeneous than comparable volumes of single crystals, because of relatively less Ca evaporation and more stable growth conditions. Hence, they often have higher T_C values for the same nominal doping. The samples were characterized using x-ray diffraction, resistivity and susceptibility. All samples were greater than 98% single phase.

4. Experimental data

The polycrystalline FM samples of (La, Ca)MnO_3 and (La, Pr, Ca)MnO_3 that we studied can be grouped into two classes (I and II) depending on the shapes of the resistivity and magnetization curves of the materials near T_C and T_{MI}. We first discuss class I materials. References [13, 19, 20] give a comprehensive summary of our μSR experiments in the class I series of polycrystalline materials $La_{1-x}Ca_xMnO_3$, $x = 0.0, 0.06, 0.18, 0.33, 0.67$ and 1.0. Our previous work on the class II $La_{5/8}Ca_{3/8}MnO_3$ material is described in [19]. Next we briefly review our findings in the $x = 0$ and 1 end members of this series, referring the reader to the literature for a more detailed discussion. The focus then will be on the FM $x = 0.18$ and 0.33 compounds.

4.1. $LaMnO_3$ and $CaMnO_3$

$LaMnO_3$ is an AFM with Néel temperature $T_N = 139$ K. The magnetic structure consists of a–b-plane FM sheets which are antiferromagnetically aligned along the c-axis. A polycrystalline sample was studied [19]. In ZF two muon frequencies having the same temperature dependence were observed below T_N corresponding to two muon sites. The spin–lattice relaxation rate $1/T_1$ was derived from good agreement with a single exponential μSR relaxation function (equation (4), with $K = 1$). A sharp AFM transition was observed, with a peak in $1/T_1$ at T_N and a temperature-independent behaviour above T_N, characteristic of spins fluctuating at their exchange frequency ω_e. The high temperature relaxation rate was found to be consistent with the mean field expression for $T_N = JzS(S+1)/3$. Here $1/T_1 \propto 1/\omega_e$, where ω_e is proportional to the exchange constant J, S is the Mn spin and z is the Mn coordination number. Thus, the ZF μSR results on $LaMnO_3$ are fully consistent with conventional spin dynamics.

$CaMnO_3$ becomes AFM at $T_N = 123$ K, exhibiting G-type AFM where each Mn atom is antiferromagnetically aligned with its nearest neighbour. Three μSR frequencies were observed below 100 K, corresponding to three muon sites, but only one frequency was found above 100 K [19]. This change in the number of observable frequencies indicates a muon site change caused by temperature-dependent activated muon hopping. As in $LaMnO_3$, $CaMnO_3$ exhibits a sharp AFM transition with a narrow peak in $1/T_1$ and a temperature-independent

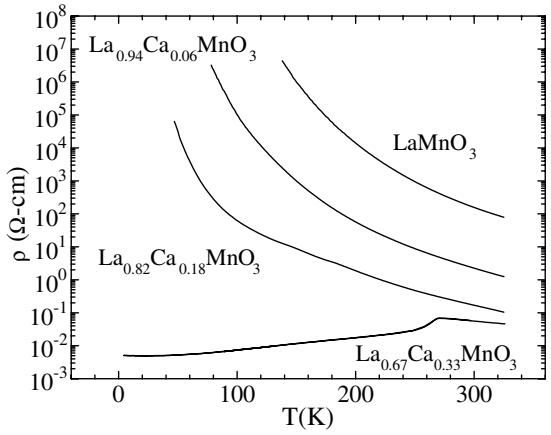

Figure 1. Temperature dependence of the resistivity for class I $La_{1-x}Ca_xMnO_3$ for $x = 0.0$, 0.06, 0.18 and 0.33.

rate above T_N. However, unlike the case of $LaMnO_3$, the data do not exhibit the mean-field agreement between T_N and $1/T_1$ above T_N. This is apparently caused by the temperature-dependent changes in muon sites.

The reader is referred to [19] for additional details and for data and discussion of the $x = 0.06$ and 0.67 compounds. A more detailed discussion of the results on the class I FM materials, $x = 0.18$ and 0.33, is presented in section 4.3 below.

4.2. Muon sites

We briefly discuss what is known about the muon sites in these materials, stressing, however, that neither the analysis of the data presented here nor the conclusions derived from these data depend on a detailed knowledge of the muon stopping sites. In undoped $LaMnO_3$ the two muon frequencies correspond to two crystallographically different sites. The first site, corresponding to the lower observed frequency in $LaMnO_3$ is very close [19, 21] to the most stable site in rare-earth orthoferrite compounds [22], which have the same crystal structure as the (La, Ca) MnO_3 materials studied here. In the orthoferrites the muon occupies three different sites at low temperatures, but only one site is stable above 100 K in $ErFeO_3$ and 300 K in $YFeO_3$, for example. In $LaMnO_3$ the most stable site is about 1 Å from the O(1) oxygen. The second site is about 1 Å from the O(2) oxygen [19]. In our sample both of these sites were found to be stable below T_N. However, experiments by others [21] showed that the second site is stable only up to 120 K. Both of the sites give the same calculated dipole hyperfine field in $La_{0.67}Ca_{0.33}MnO_3$ [19]. More definitive identification of the muon sites in these materials requires single crystals, in which not only the magnitude but also the direction of the local field can be determined.

4.3. Class I FM (La, Ca)MnO_3 materials

Figure 1 shows the resistivity $\rho(T)$ curves for the $x = 0.0$, 0.06, 0.18 and 0.33 samples measured in [19]. One sees a progressive drop in the resistivity with doping, culminating in a MI transition for $x = 0.33$, as seen by a change in slope of $d\rho/dT$ at T_{MI}. The $x = 0.18$ compound becomes FM below $T_C = 182$ K, but remains an insulator at all temperatures. The analysis of the μSR data using the stretched exponential relaxation function in equation (4) is

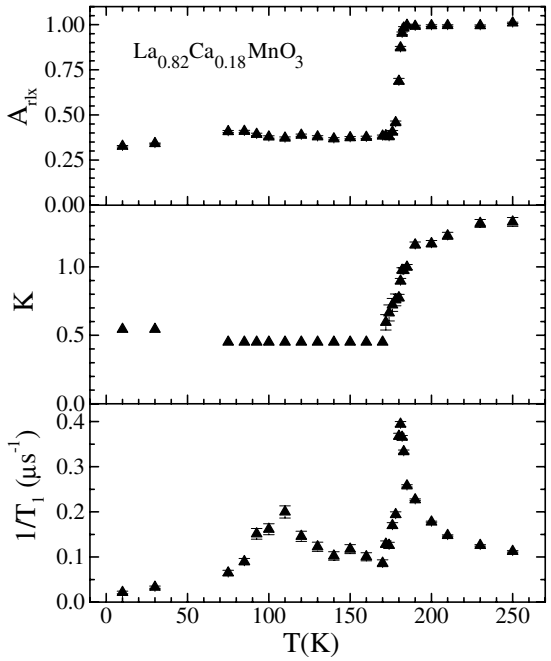

Figure 2. Temperature dependence of the μSR relaxing amplitude $A_{\rm rlx}$ (top), exponent K (middle) and spin–lattice relaxation rate $1/T_1$ (bottom) in class I $La_{0.82}Ca_{0.18}MnO_3$ from a fit to equation (4).

shown in figure 2. The FM transition is indicated by a relatively sharp peak in the temperature dependence of $1/T_1$ at 182 K, followed by a lower temperature, more gradual, maximum near 110 K. To observe this broad maximum it was necessary to freeze the value of K in the least squares fitting to equation (4) so that the form of the relaxation function would remain the same over the temperature range below about 170 K. Because μSR cannot in general determine the type of spin correlations present in these materials (this requires a momentum-dependent probe like neutron scattering), the origin of this low temperature peak is not certain. However, it is likely that it is related to the onset of some type of CO, as discussed in [19]. A single muon frequency was observed in the $x = 0.18$ material, but only for 150 K $\leqslant T \leqslant$ 180 K. The low temperature cut-off of the frequency is likely due to change in spin ordering as the system nears this putative CO state.

Figure 3 shows a similar plot for the $x = 0.33$ material, which has $T_{\rm C} \cong 270$ K and becomes metallic below $T_{\rm C}$. as seen by the resistivity in figure 1. One notices that the temperature dependence of $1/T_1$ exhibits a low-temperature 'tail' extending at least 70 K below the FM transition. As in the $x = 0.18$ material, a single, highly damped ($1/2\pi\nu T_2 \cong 0.25$) muon precession signal is observed. In the $x = 0.33$ material, however, this precession can be tracked down to the lowest measured temperatures $\cong$5 K. The onset of this precession occurs right at $T_{\rm C}$, where $A_{\rm rlx}$ also begins to deviate from its high temperature value of unity. Note, however, that $1/T_1$ has its peak at a temperature distinctly below $T_{\rm C}$ (figure 3). This is a symptom of an incorrect relaxation function having been used to fit the data. In this case, the problem is that the exponent K is temperature dependent, so that when fitting the data to the stretched-exponential form a different functional form is effectively used at each temperature. This problem can be cured (and further illuminated) as follows.

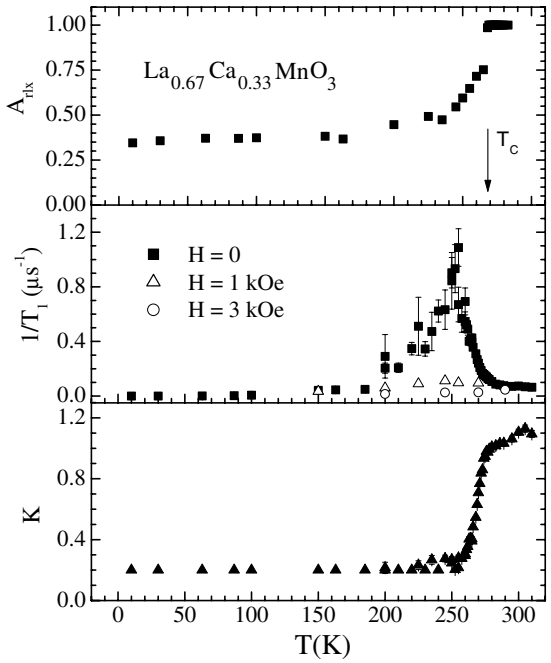

Figure 3. Temperature dependence of the μSR relaxing amplitude $A_{\rm rlx}$ (top), exponent K (middle) and spin–lattice relaxation rate $1/T_1$ (bottom) in class I $La_{0.67}Ca_{0.33}MnO_3$ from a fit to equation (4).

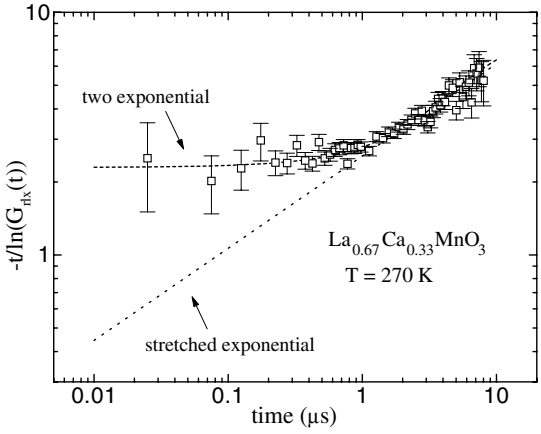

Figure 4. The measured μSR function $G_{\rm rlx}(t)$ at $T = 270$ K (open squares). The lines show calculated stretched-exponential (lower dotted line) and two-exponential (upper dashed line) functions using the fit parameters obtained from the fits shown in figure 5.

Figure 4 illustrates that the actual form of $G_{\rm rlx}(t)$ is not a stretched exponential. By plotting $-t/\ln(G_{\rm rlx})$ versus time on a log–log plot the difference between a stretched exponential and the sum of two exponentials becomes evident; the former is a straight line on such a plot (with slope $(1 - K)$) while the latter is not. Clearly the two-exponential relaxation function $G_{\rm rlx}(t)$ yields a better representation of the data.

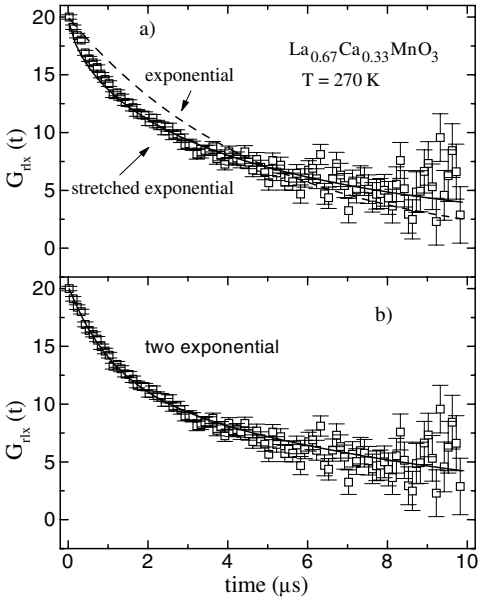

Figure 5. (a) μSR function $AG_{\rm rlx}(t)$ at $T = 270$ K. The curves show best fits using the stretched exponential in equation (4) and exponential function ($K = 1$ in equation (4)). (b) Two-exponential fit using equation (6).

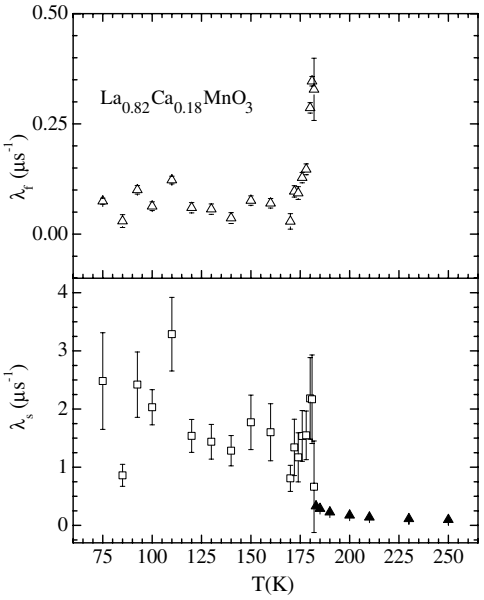

Figure 6. Temperature dependence of the μSR fast ($\lambda_{\rm f}$, top) and slow ($\lambda_{\rm s}$, bottom) spin–lattice relaxation rates for zero applied field in class I $La_{0.82}Ca_{0.18}MnO_3$ obtained from fits to equation (4) (closed symbols, exponent $K \cong 1$ in equation (4)) and equation (6) (open symbols).

A two-exponential fit to the relaxation function at $T = 265$ K for $x = 0.33$ is shown in figure 5. There is a fast relaxing rate labelled $\lambda_{\rm s}$ and a slow relaxing rate labelled $\lambda_{\rm f}$. The subscripts are chosen so that 's' stands for slowly relaxing Mn spins and 'f' stands for fast relaxing Mn spins. (Slowly fluctuating Mn spins yield a rapidly relaxing muon rate in the motional narrowing limit where $\lambda \propto \tau$.) We point out that fitting a relaxation curve to the sum of exponentials is not rigorously unique. Credible results are obtained here (and in the other cases presented) when $K < 1$ and $1/T_1 > 0.1\ \mu{\rm s}^{-1}$ because the two rates $\lambda_{\rm f}$ and $\lambda_{\rm s}$ differ by a factor of at least 10. In the case shown in figure 5 the difference is a factor of 30.

Figures 6 and 7 show the temperature dependence of the parameters $\lambda_{\rm f}$ and $\lambda_{\rm s}$ obtained from fitting $G_{\rm rlx}(t)$ to equation (6) in the $x = 0.18$ and 0.33 materials, respectively. The two-exponential fits could only be performed over a limited temperature range above and below $T_{\rm C}$, where the relaxation rate $1/T_1$ is large enough, as explained above. Sufficiently far above $T_{\rm C}$, where $K \cong 1$, the data are well represented by a single-exponential function. The open symbols correspond to the temperature region where two-exponential fits were feasible. The closed symbols at higher temperatures (bottom frames figures 6 and 7) are from the single-exponential fits. The temperature dependences of the parameters $A_{\rm f}$ and $A_{\rm s}$ are shown in figure 8.

The two-exponential fits for $x = 0.18$ and 0.33 yield very interesting results. We note that in both materials only $\lambda_{\rm f}$ peaks at $T_{\rm C}$, characteristic of the slowing down of spins near their magnetic ordering temperature. The temperature dependence of $\lambda_{\rm s}$ shows no such peak, displaying only temperature-independent behaviour below $T_{\rm C}$. Also, the relaxation rates $\lambda_{\rm f}$ and $\lambda_{\rm s}$ differ by more than an order of magnitude, with $\lambda_{\rm s} \cong 40\lambda_{\rm f}$ below $T_{\rm C}$. Using the motional-narrowing relation $\lambda = 2\omega\tau$, one may derive Mn correlation times for $La_{0.67}Ca_{0.33}MnO_3$ at

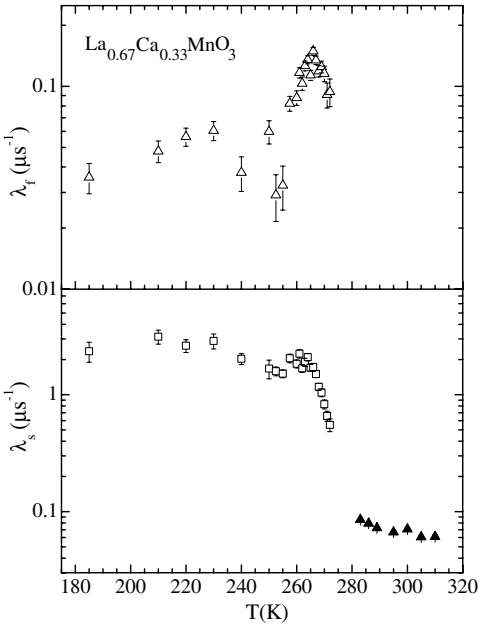

Figure 7. Temperature dependence of the μSR fast (λ_f, top) and slow (λ_s, bottom) spin–lattice relaxation rates for zero applied field in class I $La_{0.67}Ca_{0.33}MnO_3$ obtained from fits to equation (4) (closed symbols, exponent $K \cong 1$ in equation (4)) and equation (6) (open symbols).

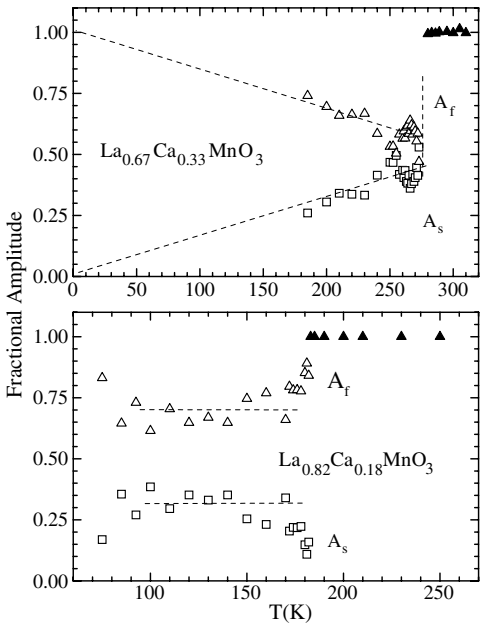

Figure 8. Temperature dependence of the μSR fast A_f and slow A_s amplitudes for zero applied field in class I $La_{0.67}Ca_{0.33}MnO_3$ and $La_{0.82}Ca_{0.18}MnO_3$ obtained from fits to equation (4) (closed symbols, exponent $K \cong 1$ in equation (4)) and equation (6) (open symbols).

$T = 250$ K, for example. One obtains $\tau_f \cong 10^{-13}$ s and $\tau_s \cong 5 \times 10^{-12}$ s, assuming that the value $\omega \cong 2\pi \times 75$ MHz measured at the lowest temperatures is representative of the muon–Mn coupling for both the slow and fast components. The ratio of amplitudes A_f/A_s near and below T_C is $\cong$3.0 for $x = 0.18$ and $\cong$1.5 for $x = 0.33$. Finally, as seen in figure 8, the amplitudes remain approximately independent of temperature below T_C in $La_{0.82}Ca_{0.18}MnO_3$, whereas A_f increases and A_s decreases below T_C in $La_{0.67}Ca_{0.33}MnO_3$.

Thus, the two FM materials $La_{0.82}Ca_{0.18}MnO_3$ and $La_{0.67}Ca_{0.33}MnO_3$ exhibit a bi-modal distribution of fluctuation rates in perhaps the most interesting part of the phase diagram. We make the reasonable assumption that the fractional sample volume corresponding to the 'slow' and 'fast' signals is given by A_s and A_f, respectively, as expected for a local probe. Therefore, this analysis is consistent with two different spatially distinguishable regions in the sample, characterized in our measurements by very different relaxation rates and temperature-dependent amplitudes. It is important to point out that, although the λ_f component may exist throughout the sample volume, the λ_s component can only exist in spatially separated regions. If this were not true only the slow Mn fluctuation rate (which creates the largest μSR rate) would be observed. The muon samples these separate regions locally through its relatively short-ranged dipolar coupling to the Mn spins (matrix element $\sim r^{-6}$).

Note that neither relaxation component corresponds to the relaxation rate in pure $LaMnO_3$ or $CaMnO_3$, whose relaxation rates are independent of temperature above 140 K with magnitudes $\cong$0.1–0.05 μs^{-1} [19]. This argues against large-scale separation of Mn^{3+} and Mn^{4+} ions.

This inhomogeneity in the spin channel is frozen in the insulating $x = 0.18$ material, where A_s and A_f remain relatively independent of temperature below T_C. For the $x = 0.33$

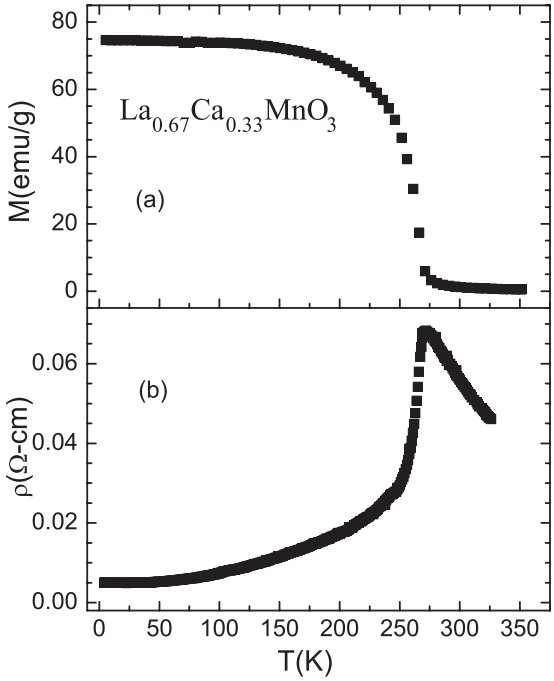

Figure 9. Temperature dependence of (a) magnetization in 2 kOe applied field and (b) resistivity in zero applied field of class I polycrystalline $La_{0.67}Ca_{0.33}MnO_3$.

metallic material the fast fraction given by A_f becomes more predominant at low temperatures. Indeed, this fraction extrapolates to 1 at $T = 0$, as seen in figure 8. Therefore, we arrive at the hypothesis that the 'fast' and 'slow' components arise from spatially separated conducting and insulating regions in the samples, respectively. This hypothesis means that even in the metallic state of these polycrystalline materials there exist sizeable pockets of insulating material far below T_C.

4.4. Class II FM materials

To test this hypothesis and explore these materials further a new series of experiments on polycrystalline FM CMR manganites was carried out. The results reported here were performed on a sample of $La_{5/8}Ca_{3/8}MnO_3$ whose resistivity and magnetization curves were distinctly different from the class I $x = 0.33$ material discussed above. Note that $x = 3/8$ is the Ca composition that yields the maximum $T_C = 273$ K for the (La, Ca)MnO_3 series of compounds [15]. Figures 9 and 10 show the resistivity $\rho(T)$ and susceptibility $\chi(T)$ for these two classes of materials. The resistivity of the class II material shows a distinct low-temperature 'bump' below $T_{MI} \cong T_C$, as well as a steeper temperature dependence above T_{MI}. The maximum in the resistivity occurs at $T_{MI} = 273 \pm 1$ K, a signature of the MI transition. The susceptibilities of the two samples are also different. Whereas the class I sample has a rounded, mean-field-like temperature dependence, the $\chi(T)$ of the class II sample looks more first order near T_C. The inflection point of $\chi(T)$ occurs at $T_C = 272 \pm 1$ K, indicating that $T_{MI} = T_C$ in this sample. We also carried out extensive μSR measurements on a second class II $x = 0.33$ sample. The results were very similar to those for the $x = 3/8$ sample described next and are, therefore, not presented here. It is important to point out that both the class I

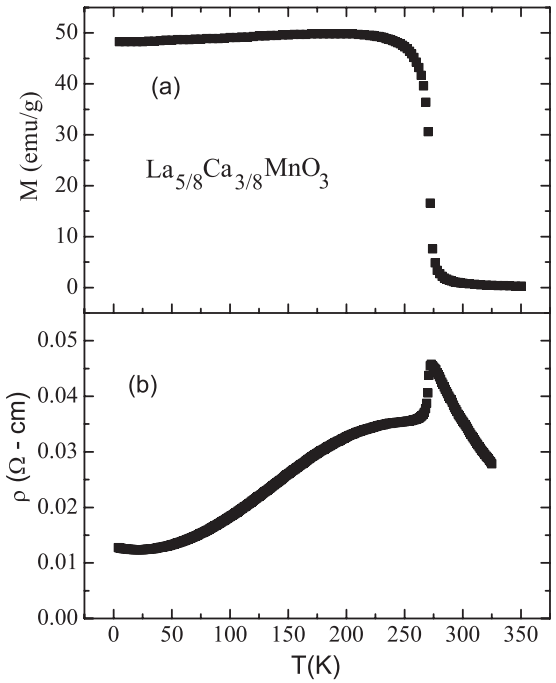

Figure 10. Temperature dependence of (a) magnetization in 1 kOe applied field and (b) resistivity in zero applied field of class II polycrystalline $La_{5/8}Ca_{3/8}MnO_3$.

and class II materials were considered to be 'state-of-the-art' polycrystalline (La, Ca)MnO_3 materials at the time of their measurement. Indeed, the class II material studied here is still regarded in this fashion.

We now describe the ZF μSR results on the $x = 3/8$ sample. The oscillating and relaxing terms of the relaxation function $G_z(t)$ at and below T_C were well described by equations (3) and (6), respectively, yielding two exponential relaxation rates $\lambda_f(T)$ and $\lambda_s(T)$, as described above. The parameters A_O and A_R were consistent with a polycrystalline average, $A_O \cong 2/3$ and $A_R \cong 1/3$. Above T_C $G_{rlx}(t)$ is well described by a single exponential with rate $\lambda_e(T)$. The data are consistent with only a single resolvable μSR frequency $\nu(T)$, as found for the class I FMs described above. The linewidth $1/2\pi\nu T_2 \cong 0.2$–0.3 was found to be independent of temperature.

Figure 11(a) shows the temperature dependence of $\nu(T)$, together with a fit (solid curve) to the expression $\nu(T) = (1 - T/T_C)^{\beta}$, often used to describe the magnetization of FM materials. We find $\beta = 0.28 \pm 0.01$ and $T_C = 271.8 \pm 0.4$ K. The value of β is somewhat smaller than found for the class I $x = 0.33$ material discussed above (where $\beta = 0.34$). This smaller value of β indicates a more nearly first-order behaviour. Note that neither these fits nor the fits to the $x = 0.33$ material give a real 'critical exponent', which can only be derived from measurements very close to T_C, preferably on single crystals. Nonetheless, a comparison of β values is useful to characterize the different materials. It is noteworthy that the fitted value for T_C from the $\nu(T)$ data is fully consistent with the resistivity and susceptibility measurements.

Figures 11(b) and (c) display the temperature dependence of λ_s, λ_e and λ_f. We were able to perform a two-exponential fit in the temperature range 85 K $\leqslant T \leqslant$ 273 K. At lower temperatures the overall relaxation rate is too small; above 273 K the data are consistent with

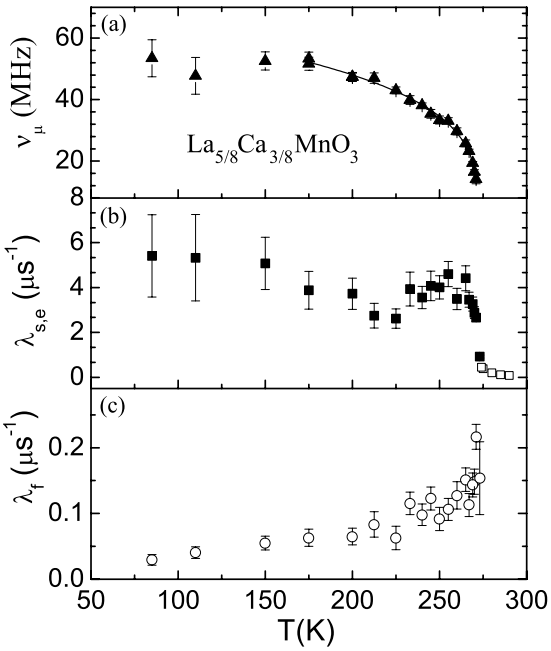

Figure 11. Temperature dependence of (a) the spontaneous precession frequency, (b) slow (filled squares) and single-exponential (open squares) μSR rates, and (c) fast μSR rates from fits to equation (6) in class II $La_{5/8}Ca_{3/8}MnO_3$. The solid curve in (a) is a fit to $\nu(T) = (1 - T/T_C)^\beta$, as described in the text.

single-exponential relaxation. The ratio of λ_s/λ_f is between 10 and 100. The onset of two-exponential relaxation thus occurs right at $T_C \cong T_{MI}$, as defined by the susceptibility and resistivity data, as well as the fitted T_C from the $\nu(T)$ curve in figure 11(a). Note that there is no peak in the temperature dependence of λ_f, unlike in the $x = 0.33$ class I sample. This seems to reflect the sharper onset of the FM transition as seen in the $\chi(T)$ data. Except for this, the overall behaviour of the $x = 3/8$ data is very similar to the $x = 0.33$ class I data.

Figure 12 displays the temperature dependence of the two amplitudes A_f and A_s for $x = 3/8$. Here the sharper transition in the class II sample enables a more definitive interpretation of the data. Note that the temperature dependences of $A_s(T)$ and $A_f(T)$ are relatively gradual below about 265 K, where $A_s(T)$ trends towards zero and $A_f(T)$ trends towards unity at $T = 0$ (dotted lines in figure 12). Between 265 K and $T_{MI} = 273$ K, however, the temperature dependences are more rapid, with $A_s(T)$ trending towards 1 and $A_f(T)$ trending towards zero. This implies that the slow component connects smoothly with the single-exponential relaxation above T_{MI}, where the sample is insulating. Indeed, the rate λ_e extrapolates smoothly to λ_s at T_{MI}, as seen in figure 11(b). The temperature dependences of the amplitudes are therefore consistent with associating the 'slow' and 'fast' components with insulating and conducting regions of the sample below T_C, which is fully consistent with our hypothesis based on the data from the more inhomogeneous class I FM samples.

4.5. $La_{0.35}Pr_{0.35}Ca_{0.30}MnO_3$: $T_{MI} \neq T_C$

The following question arises: is the onset of two relaxation channels related to the metal insulator transition or to the FM transition? This cannot be answered from the studies discussed

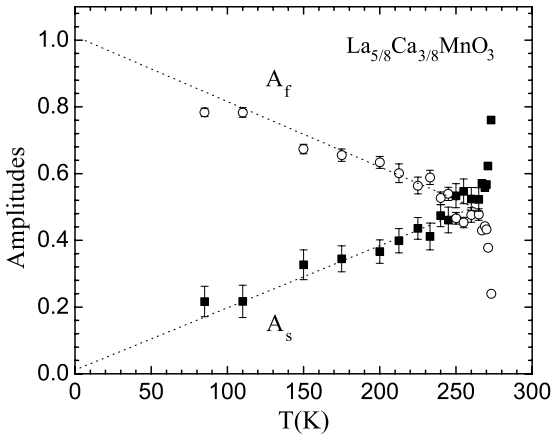

Figure 12. Temperature dependence of the slow and fast μSR amplitudes from fits to equation (6) in class II $La_{5/8}Ca_{3/8}MnO_3$. The dotted lines are guides to the eye.

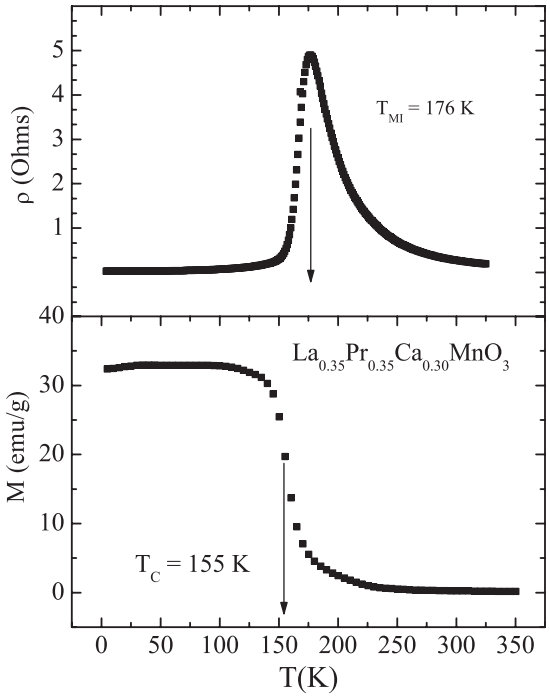

Figure 13. (a) Temperature dependence of the resistivity $\rho(T)$ and (b) magnetization $M(T)$ in 1 kOe applied field for $La_{0.35}Pr_{0.35}Ca_{0.30}MnO_3$. The maximum in $\rho(T)$ (arrow) occurs at $T_{MI} = 176$ K, indicating the MI transition. (Sometimes T_{MI} is taken to be the maximum in $d\rho/dT = 166$ K.) The inflection point in $\chi(T)$ occurs at $T_C = 155$ K.

above where $T_{MI} \cong T_C$. In the compound $La_{0.35}Pr_{0.35}Ca_{0.30}MnO_3$, however, the resistivity maximum $T_{MI} = 176$ K whereas $T_C = 155$ K. This is illustrated in figure 13, which shows the $\rho(T)$- and $\chi(T)$-data for $La_{0.35}Pr_{0.35}Ca_{0.30}MnO_3$. T_C is depressed considerably from $La_{0.70}Ca_{0.30}MnO_3$ ($T_C \cong 260$ K), though both have 30% Ca doping because of the A-site

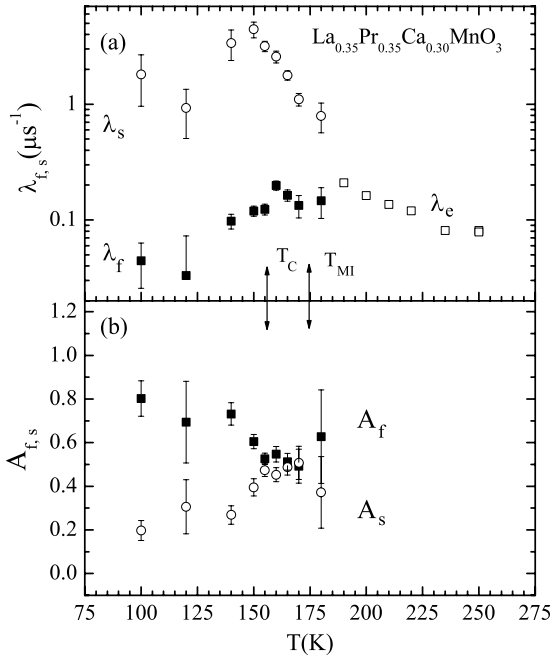

Figure 14. Temperature dependence of (a) the fast λ_f, slow λ_s and single-exponential λ_e μSR rates, and (b) the relative amplitudes A_f and A_s using a two-exponential form (equation (6)) in $La_{0.35}Pr_{0.35}Ca_{0.30}MnO_3$. The vertical double arrows show the Curie (T_C) and MI (T_{MI}) transitions.

disorder and the ionic size effect [16] in the ABO_3 perovskites. The ionic radii of Pr^{3+} and Ca^{2+} are about the same, $\widetilde{=}1.18$ Å, which is considerably smaller than La^{3+} ($\widetilde{=}1.22$ Å). This produces greater relative distortion in $La_{0.35}Pr_{0.35}Ca_{0.30}MnO_3$ than in $La_{0.70}Ca_{0.30}MnO_3$. These distortions, and the greater disorder, depress T_C by reducing the hole mobility between Mn^{4+} and Mn^{3+} and increasing the effective electron–phonon coupling [6, 16]. Thus, T_C occurs well below the onset of conductivity in $La_{0.35}Pr_{0.35}Ca_{0.30}MnO_3$.

The ZF μSR data on $La_{0.35}Pr_{0.35}Ca_{0.30}MnO_3$ were fitted in the same way as for the previous samples. We were unable to observe an oscillating component in $La_{0.35}Pr_{0.35}Ca_{0.30}MnO_3$, most likely because of the increased disorder in this material. Figure 14 shows the relaxation rate data λ_s, λ_f and λ_e, as well as the amplitudes for the 'slow' and 'fast' relaxation channels [20]. Two distinct relaxation channels are resolvable only in the temperature range 100 K $\leqslant T \leqslant$ 180 K. Below 100 K the overall relaxation rate is too small to fit to two separate components. The upper temperature 180 K is close to T_{MI} and considerably above T_C, which immediately answers our question: two separate relaxing channels are opened up at the MI transition and not at the FM transition. Furthermore, since the system is clearly insulating above T_{MI}, it is the formation of conducting regions below T_{MI} that provides the second 'fast' relaxation channel. Note that the two amplitudes A_f and A_s are comparable in the region 150 K $\leqslant T \leqslant$ 180 K, indicating that only about half of the sample becomes conducting between T_{MI} and T_C. Furthermore, associating A_f with the conducting regions, as before, one sees that the fractional volume of these regions increases below T_C. This temperature is also approximately where both λ_s and λ_f reach a maximum (figure 14(a)). We note that impedance spectroscopy measurements carried out in $La_{0.30}Pr_{0.4}Ca_{0.30}MnO_3$ find a high-frequency and a low-frequency component, evidence for two well defined bulk contributions to the transport properties below T_{MI} [23].

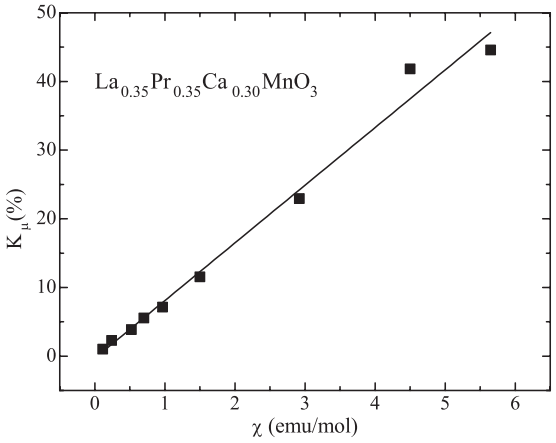

Figure 15. Knight shift constant K_μ versus bulk susceptibility in $La_{0.35}Pr_{0.35}Ca_{0.30}MnO_3$. The solid line is a fit yielding a hyperfine field of 469 ± 20 Oe/μ_B.

We also performed TF experiments on this material in an applied field of about 0.1 T. The sample was mounted on a Ag backing so that the muon beam stopped in both the $La_{0.35}Pr_{0.35}Ca_{0.30}MnO_3$ and the Ag. The resulting two-frequency spectrum was fitted according to equation (7) with exponential relaxation rates $1/T_{2i}$ and precession frequencies ν_i ($i = 1, 2$) for the $La_{0.35}Pr_{0.35}Ca_{0.30}MnO_3$ and Ag materials, respectively.

One quantity of interest from such measurements is the local susceptibility, which is derived from the Knight shift constant K [17],

$$K = K_\mu + K_{\rm dem} = (\nu_1 - \nu_2)/\nu_2, \tag{8}$$

where $K_{\rm dem}$ is the shift due to the Lorentz and demagnetization fields, as described in [17], and

$$K_\mu = [H_0\chi_0 + H_{\rm hyp}\chi_{\rm df}(T)]/N_A\mu_B. \tag{9}$$

In equation (9) $H_{\rm hyp}$ is the hyperfine field between the muon and the Mn moments, N_A is Avogadro's number and μ_B is the Bohr magneton. The molar susceptibility is used in equation (9), consisting of a temperature-independent component χ_0 (with hyperfine coupling H_0) and a component which reflects the T-dependence of the Pr and Mn moments $\chi_{\rm df}(T)$. Note that the relevant susceptibility in a Knight shift measurement is the local susceptibility in the vicinity of the muon site.

The Knight shift constant K_μ is plotted versus χ (bulk) in figure 15 for $149\ {\rm K} \leqslant T \leqslant 250\ {\rm K}$ (with temperature as an implicit parameter). One sees that K_μ scales with the measured bulk susceptibility as expected. A hyperfine field $H_{\rm hyp} = 469 \pm 20$ Oe/μ_B is extracted from the slope of the K_μ–χ data. Figure 16 shows the temperature dependence of the quantity $W = 1/(K_\mu 2\pi\nu_1 T_2)$, which is the fractional linewidth for the $La_{0.35}Pr_{0.35}Ca_{0.30}MnO_3$ signal ($1/2\pi\nu_1 T_2$) divided by the Knight shift constant. If the linewidth just scales with χ, as might be expected for a polycrystalline material, W should be independent of temperature. Instead, W is constant only well above $T_{\rm MI}$; at $T \lesssim T_{\rm MI}$ there is an abrupt decrease in W, which decreases even faster below T_C. Evidently, the opening of a conducting channel in $La_{0.35}Pr_{0.35}Ca_{0.30}MnO_3$ causes a relative narrowing of the overall inhomogeneous, static linewidth in the presence of an applied field. (The fact that this change begins above $T_{\rm MI}$ is most likely due to chemical inhomogeneities in the five-element compound.) It is plausible

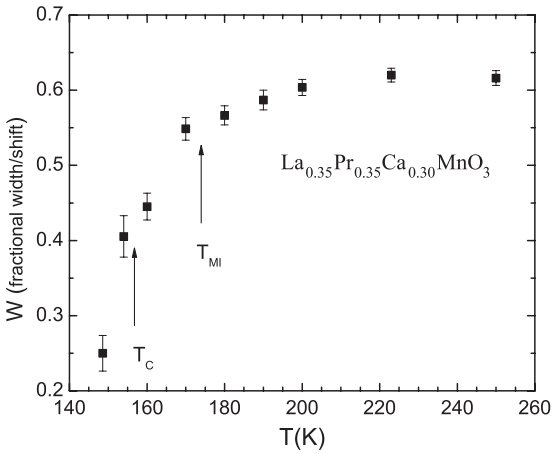

Figure 16. The fractional transverse linewidth W (see text) versus temperature in $La_{0.35}Pr_{0.35}Ca_{0.30}MnO_3$.

that this narrowing occurs because the spins in the conducting, FM regions are more easily aligned by the applied field.

4.6. Single-crystalline $La_{0.75}Ca_{0.25}MnO_3$

A single crystal of $La_{0.75}Ca_{0.25}MnO_3$ was obtained from Oak Ridge National Laboratory for ZF μSR studies[5]. This sample is the same as used previously for inelastic neutron scattering experiments [24], and was in the approximate form of a cylindrical boule with the c-axis along the cylinder axis. The initial muon polarization was approximately normal to the cylinder axis; no attempt was made to align the muon polarization along any particular crystalline direction. The Curie temperature for this material is about $T_C = 190$ K $\cong T_{MI}$ [24], somewhat lower than obtained with polycrystalline samples of the same composition.

The relaxing ZF signal $G_{rlx}(t)$ was first fitted to the stretched exponential form in equation (4); the temperature dependence of the amplitude, spin–lattice relaxation rate $1/T_1$ and exponent K are shown in figure 17. The μSR data reflect a reasonably sharp transition, as seen by the changes in all three quantities at T_C. In particular, the relaxing amplitude A_{rlx} falls sharply to its constant low-temperature value just below T_C. Note that, compared to the class I and II polycrystalline materials discussed above, the relaxation rate $1/T_1$ drops off sharply below T_C.

The fits to the two-exponential relaxation function (equation (6)) below $T_C = T_{MI}$ and the single-exponential function with rate λ_e above T_{MI} are shown in figure 18. The fast rate λ_f drops to its minimum value $\leqslant 0.01\ \mu s^{-1}$ as the temperature is decreased by 15–20 K below T_{MI}. The slow amplitude A_s reaches a value of $\leqslant 5\%$ over the same decreasing temperature range. Thus, although there are clearly two well resolved relaxation channels in this single-crystal sample for $0\ \text{K} \leqslant (T_C - T) \leqslant 90$ K, the strength of the slow, insulating component dies off more rapidly with temperature than in either the class I or class II polycrystals. This seems to be a progressive trend, with the 'slow' relaxation component dying off more rapidly at temperature below T_{MI} as one progresses from the class I to the class II to the single-crystal FM materials.

[5] We thank Dr Pencheng Dai from Oak Ridge National Laboratory for loaning us this sample.

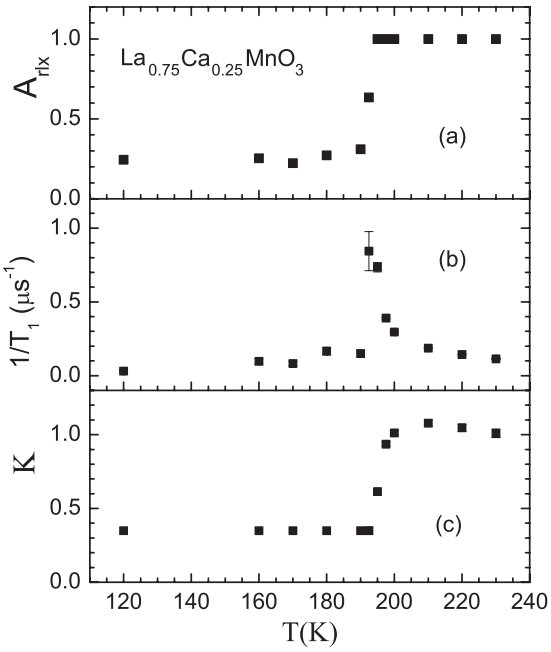

Figure 17. (a) Temperature dependence of the relaxing amplitude $A_{\rm rlx}$, (b) spin–lattice-relaxation rate $1/T_1$ and (c) exponent K from fits to the μSR function using a stretched-exponential form (equation (4)) in single-crystal $La_{0.75}Ca_{0.25}MnO_3$.

5. Discussion and conclusions

This paper has focused on the discovery of two relaxation channels below the MI transition in the CMR manganite series (La, Ca, Pr)MnO_3. μSR experiments were reported on both insulating and conducting FM materials, ranging from the earliest studied polycrystalline materials (class I), to polycrystalline materials produced later in time (class II), and finally to a single crystal of $La_{0.75}Ca_{0.25}MnO_3$ studied previously by neutron scattering. In the class II granular materials the temperature dependences of the susceptibility and resistivity indicated the FM and MI transitions were sharper than in the class I granular materials—appearing almost first order. We also carried out experiments on polycrystalline $La_{0.35}Pr_{0.35}Ca_{0.30}MnO_3$ in which $T_C \cong T_{MI} - 20$ K, unlike the class I, class II and single-crystal FMs where $T_C \cong T_{MI}$.

The experiments in the metallic CMR FMs $La_{1-x}Ca_xMnO_3$, with $x = 0.33$ and 0.375, are consistent with the opening of two relaxation channels at $T_C \cong T_{MI}$. There is a slowly relaxing component ($\tau \cong 5 \times 10^{-12}$ s) with a decreasing volume fraction below T_C, and a more rapidly relaxing component ($\tau \cong 10^{-13}$ s) with an increasing volume fraction below T_C, which extrapolates to about 100% as the temperature approaches zero. Experiments in $La_{0.35}Pr_{0.35}Ca_{0.30}MnO_3$ confirmed that the onset of the 'fast' relaxation channel in μSR is to be associated with the opening of conducting regions in these materials below T_{MI}. The growth of this fast component's amplitude A_f in $La_{0.35}Pr_{0.35}Ca_{0.30}MnO_3$ occurs only as the temperature is reduced below T_C where the material becomes more and more metallic. By contrast, A_f and A_s are *independent of temperature* in $La_{0.35}Pr_{0.35}Ca_{0.30}MnO_3$ for all $T_C \leqslant T \leqslant T_{MI}$, e.g., in the *insulating* state. This is similar to the $x = 0.18$ *insulating* FM where both A_f and A_s remain independent of temperature for $T \leqslant T_{MI} = T_C$. In this material the onset of FM, associated with increased hole mobility, is not sufficient to increase the conducting volume

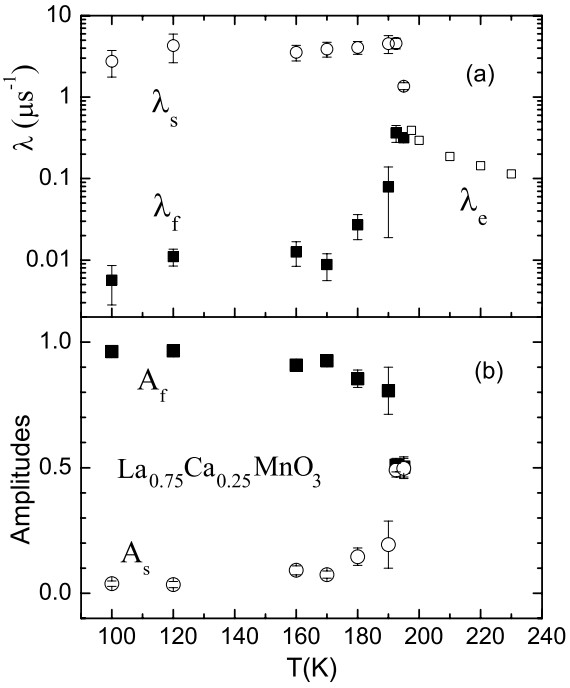

Figure 18. Temperature dependence of (a) the fast λ_f, slow λ_s and single-exponential λ_e μSR rates, and (b) the relative amplitudes A_f and A_s using a two-exponential form (equation (6)) in single-crystal $La_{0.75}Ca_{0.25}MnO_3$.

fraction even far below T_C because the concentration of doped holes is still relatively low. In $La_{0.35}Pr_{0.35}Ca_{0.30}MnO_3$, however, where both the hole concentration and the local lattice distortions (which retard hole mobility) are larger, a conducting path opens up at T_{MI}, but the hole mobility is presumably not large enough to increase the average fractional conducting volume until the temperature is lowered still further below T_C. Only then (at $T < T_C$) do we find that A_f increases and A_s decreases with lowered temperature. Thus, the nature of a local spin probe like μSR yields insight into the microscopic growth of conducting regions in these CMR materials as the system becomes more and more metallic with decreasing temperature.

We point out that our results are consistent with other measurements which also point to an intrinsic difference between granular and crystalline CMR materials. First, neutron pair distribution function measurements, which measure the relative fraction of Mn–O Jahn–Teller distorted (insulating) and non-distorted (conducting) regions in these materials, find a roughly 50% fractional volume of conducting regions at T_C which increases only gradually with decreasing temperature in polycrystalline (La, Ca)MnO_3 ferromagnets [25]. Second, a non-exponential μSR relaxation was also found in a *narrow* temperature region below T_C in *single crystals* of the bi-layer manganites [26], consistent with the single-crystal results discussed above for $La_{0.75}Ca_{0.25}MnO_3$. Finally, we also point out that complementary information concerning the inhomogeneous nature of these materials has also been found from NMR experiments [12].

Possible additional confirmation for our picture can be obtained by examining the magnitude of the two relaxation rates, noting that they differ by a factor of 30–50. Neutron scattering experiments in which the spin-wave stiffness constants D_{SW} were measured for both insulating and conducting $La_{1-x}Ca_xMnO_3$ compounds found that D_{SW} is about three times

larger in the metallic materials than in the insulators [24]. The low-temperature μSR rate from relaxation due to spin waves occurs via a two-magnon process which is proportional to D_{SW}^{-3} [27]. Thus, the low-temperature μSR relaxation from this mechanism in FM insulating regions should be about 30 times faster than from FM conducting regions. This is certainly consistent with our assignment of λ_f and λ_s. We also note that the growth of FM order parameters with similar temperature dependences in both insulating and conducting regions is supported by the observation of only a single, broad oscillating μSR signal. However, the observed low-temperature magnitude of D_{SW} is large [24, 28], meaning that one would *not* expect significant low-temperature relaxation of the muon's spin from this mechanism [13]. Indeed, our observed μSR rates at the lowest temperatures are negligible, as expected. Therefore, the λ_f and λ_s rates which we do observe are likely caused by higher-order magnon relaxation processes arising from over-damped spin waves. Why *over-damped* spin waves? Note that inelastic neutron scattering experiments see only a single spin wave component below T_C. One may postulate, therefore, that the insulating regions which we observe are filamentary, so that each such region possesses a very small individual volume which is too small to support spin waves (i.e., their characteristic dimensions are less than the spin–spin correlation length), even though all together they occupy a sizeable fraction of the sample volume near T_C.

A crucial question still remains: what is the origin of the insulating and conducting regions in these materials? Evidence strongly suggests that in granular CMR materials regions of drastically different conductivity originate from the conducting cores of the grains and their surrounding insulating layers. The strongest evidence for this assertion comes from systematic studies of the magnetization and resistivity as a function of grain size. Grain size can be measured using x-ray diffraction and can be varied by changing the sample preparation protocol: a higher sintering temperature yields larger average grain sizes, for example. In general, samples of (La, Ca)MnO_3 with larger grains have more first-order looking (sharper) magnetization versus temperature curves [29]. NMR data at 4.2 K in FM (La, Ca)MnO_3 show both a strong resonance characteristic of $Mn^{3+/4+}$ in metallic regions and a less intense, lower frequency resonance line characteristic of insulating regions of Mn^{4+} [29]. The intensity of this lower frequency resonance grows as the grain size is reduced, indicating a greater surface-to-volume ratio for the insulating regions associated with Mn^{4+}. Model calculations [30] of the tunnelling resistivity across grains using a picture of conducting granular cores surrounded by insulating shells are also able to reproduce the bump in the resistivity seen below T_C in some granular CMR materials (see figure 10, for example).

We can estimate the overall impact of this picture on the μSR data. Assuming spherical grains of total diameter L with an insulating shell of thickness w, the fractional volume of the conducting regions, assuming a 100% packing factor, is simply $(L-2w)^3/L^3 \cong 1-6w/L$ for $w \ll L$. It is generally agreed that $w \cong 2$ nm [29, 30]. We measured $A_f \cong 50$–75% of the sample volume near T_C, which would be consistent with grain sizes $L \cong 25$–50 nm (for $w \cong 2$ nm) in our granular materials. The magnetization for our class I $x = 0.33$ FM material is about 90 emu g^{-1} at an applied field of 1.8 T, well into the saturation region. The magnetization at low temperatures in 1–2 kOe applied fields for the class I and II materials shown in figures 9 and 10, together with the saturation value of 90 emu g^{-1}, are all consistent with grain sizes $\geqslant$1000 nm, as shown in [29]. Thus, this picture cannot account for the relatively large insulating volume fraction measured by μSR in the polycrystals, and one must find another source for the differences between the crystalline and polycrystalline data. Thus, these materials possess intrinsic inhomogeneities which are not yet understood and point to the importance of complexity and competing phases and interactions in CMR manganites.

Our findings could have important implications for the use of CMR materials in magnetoresistive devices. The tunnelling magnetoresistance can be used as a tuning parameter

in CMR-based multilayers, for example [10]. A highly spin-polarized current from a magnetized layer is forced to tunnel through an insulating junction into a second magnetized layer. One or both of the magnetic layers can be a CMR material. The low resistivity state of these tunnel junctions occurs when the two magnetic layers are magnetized in the same direction. This situation can be switched from a high resistance to a low resistance state with a magnetic field, if the two layers have sufficiently different coercive fields. Typically the tunnel junction material is $\leqslant$10–20 Å thick. Clearly, if the CMR films have insulating regions near their surfaces, the effective thickness of the tunnel junction is increased, resulting in an exponentially decreasing tunnelling current. Polarized x-ray experiments probing different depths of (La, Sr) MnO_3 films did indeed find depth-dependent magnetization curves, indicating a non-metallic layer at the film's surface [31]. Our μSR experiments provide additional evidence for insulating regions below T_C even in bulk materials. In addition, μSR is the first probe to convincingly measure the temperature dependence of the insulating fraction, together with its associated spin–lattice relaxation rate, in CMR materials. In this regard, we point out that to measure relaxation times $\tau \cong 5 \times 10^{-12}$ s with inelastic neutron scattering requires a resolution $\ll$1 meV, below the resolution of most triple-axis spectrometers.

Acknowledgments

We thank G Balakrishnan, S-W Cheong, J S Gardner, M F Hundley, G M Luke, T Kimura, K Kojima, L P Le, J F Mitchell, B Nachumi, J J Neumeier, William Ratcliff II, J S Sarrao, J D Thompson, Y Tokura and Y J Uemura for participation in the μSR experiments reviewed here. We also thank the μSR facilities' personnel who helped to make this work possible: A Amato, D Arsenau, C Baines, M Good, D Herlach, B Hitti, S Kreitzman and U Zimmermann. We also acknowledge helpful discussions with P Dai, J Fernandez-Baca, J Lynn, A Millis, R Osborn, M Salamon, A J Taylor and S Trugman. Research reported here was performed in part under the auspices of the US DOE (Los Alamos) and supported in part by the US NSF, grant no DMR-0102293 (Riverside), the Netherlands NWO and FOM (Leiden) and the Canadian NSERC (Burnaby).

References

[1] Jonker G H and van Santen J H 1950 *Physica* **16** 337
Wollen E O and Koehler W C 1955 *Phys. Rev.* **100** 548
[2] Zener C 1951 *Phys. Rev.* **82** 403
Anderson P W and Hasegawa H 1955 *Phys. Rev.* **100** 675
deGennes P G 1960 *Phys. Rev.* **118** 141
[3] Goodenough J B 1995 *Phys. Rev.* **100** 564
Kanamori J 1959 *J. Phys. Chem. Solids* **10** 87
[4] Tokura Y (ed) 2000 *Colossal Magnetoresistive Oxides* (*Advances in Condensed Matter Science* vol 2) (The Netherlands: Gordon and Breach)
[5] Louca D, Egami T, Brosha E L, Röder R and Bishop A R 1997 *Phys. Rev.* B **56** R8475
Billinge S J L and Proffen T 2002 *Appl. Phys.* A **74** S1770
Booth C H, Bridges F, Kwei G H, Lawrence J M, Cornelius A L and Neumeier J J 1998 *Phys. Rev. Lett.* **80** 853
[6] Mathur N D and Littlewood P B 2001 *Solid State Commun.* **119** 271
Dagotto E, Hotta T and Moreo A 2001 *Phys. Rep.* **344** 1
Millis A J, Littlewood P B and Shraiman B I 1996 *Phys. Rev.* B **54** 5389
Millis A J, Littlewood P B and Shraiman B I 1996 *Phys. Rev.* B **54** 5405
Roder H, Zang J and Bishop A R 1996 *Phys. Rev. Lett.* **76** 1356
[7] Murakami Y, Kawada H, Kawata H, Tanaka M, Arima T, Moritomo Y and Tokura Y 1998 *Phys. Rev. Lett.* **80** 1932
Kondo H, Ishihara S and Maekawa S 2001 *Phys. Rev.* B **64** 014414

[8] Mori S, Chen C H and Cheong S-W 1998 *Nature* **392** 473
Radaelli P G, Cox D E, Marezio M and Cheong S-W 1997 *Phys. Rev.* B **55** 3015
Chen C H and Cheong S-W 1996 *Phys. Rev. Lett.* **76** 4042
[9] Nadgorny B, Mazin I I, Osofsky M, Soulen R J Jr, Proussard P, Stroud R M, Singh D J, Harris V, Arsenov A and Mukovskii Ya 2001 *Phys. Rev.* B **63** 184433
[10] Gupta A and Sun J Z 1999 *J. Magn. Magn. Mater.* **200** 24
O'Donnell J, Andrus A E, Oh S, Colla E V and Eckstein J N 2000 *Appl. Phys. Lett.* **76** 1914
Ogimoto Y, Izumi M, Sawa A, Manako T, Sato H, Akoh H, Kawasaki M and Tokura Y 2003 *Japan. J. Appl. Phys.* **42** L369
[11] Moussa F, Biotteau G, Hennion M, Rodriguez Carvajal J, Pinsard L and Revcolevschi A 1999 *J. Supercond.* **12** 257
[12] Allodi G, Guidi M C, De Renzi R and Pieper M W 2002 *J. Magn. Magn. Mater.* **242–245** 635
Allodi G, Cestelli Guidi M, De Renzi R and Caniero A 2001 *Phys. Rev. Lett.* **87** 127206
De Renzi R, Allodi G, Amoretti G, Guidi Cestelli M, Fanesi S, Guidi G, Licci F, Caneiro A, Prado F, Sanchez R, Oseroff S and Amato A 2000 *Physica* B **289/290** 85
[13] Heffner R H, Sonier J E, MacLaughlin D E, Nieuwenhuys G J, Ehlers G, Mezei F, Cheong S-W, Gardner J S and Röder H 2000 *Phys. Rev. Lett.* **85** 3285
[14] Garcia-Munoz J L, Llobet A, Frontera C and Ritter C 1999 *J. Appl. Phys.* **85** 5639
Barsov S G 2000 *Physica* B **289/290** 81
De Teresa J M, Ibara M R, Algarabel P, Morellon L, Garcia-Landa B and Marquina C 2002 *Phys. Rev.* B **65** 100403
[15] Cheong S-W and Hwang H Y 2000 *Colossal Magnetoresistive Oxides* (*Advances in Condensed Matter Science* vol 2) ed Y Tokura (The Netherlands: Gordon and Breach)
[16] Hwang H Y, Cheong S-W, Radaelli P G, Marezio M and Batlogg B 1995 *Phys. Rev. Lett.* **75** 914
[17] Schenck A 1985 *Muon Spin Rotation Spectroscopy: Principles and Applications to Solid State Physics* (Bristol: Hilger)
[18] Istratov A A and Vyvenko O F 1999 *Rev. Sci. Instrum.* **70** 1233
[19] Heffner R H, Sonier J E, MacLaughlin D E, Nieuwenhuys G J, Luke G M, Uemura Y J, Ratcliff W II, Cheong S-W and Balakrishnan G 2001 *Phys. Rev.* B **63** 094408
[20] Heffner R H, Sonier J E, MacLaughlin D E, Nieuwenhuys G J, Mezei F, Ehlers G, Mitchell J F and Cheong S-W 2003 *Physica* B **326** 494
[21] De Renzi R, Allodi G, Guidi Cestelli M, Guidi G, Hennion M, Pinsard L and Amato A 2000 *Physica* B **289/290** 52
[22] Holzschuh E, Denison A B, Kundig W, Meier P F and Patterson B D 1983 *Phys. Rev.* B **27** 5294
[23] Souza J A, Jardim R F, Muccillo R, Muccillo E N S, Torikachvili M S and Neumeier J J 2001 *J. Appl. Phys.* **89** 6636
[24] Dai P, Fernandez-Baca J A, Plummer E W, Tomioka Y and Tokura Y 2001 *Phys. Rev.* B **64** 224429
[25] Billinge S J L 2004 *Workshop on 'CMR Manganites and Related Transition Metal Oxides' (Telluride, CO)* unpublished
[26] Heffner R H, MacLaughlin D E, Nieuwenhuys G J, Kimura T, Luke G M, Tokura Y and Uemura Y J 1998 *Phys. Rev. Lett.* **81** 1706
Coldea A I, Blundell S J, Steer C A, Mitchell J F and Pratt F L 2002 *Phys. Rev. Lett.* **89** 277601
[27] Lovesey S W 1992 *J. Phys.: Condens. Matter* **4** 2043
Dalmas de Reotier P and Yaouanc A 1995 *Phys. Rev.* B **52** 9155
[28] Lynn J W, Erwin R W, Borchers J A, Huang Q, Santoro A, Peng J-L and Li Z Y 1996 *Phys. Rev. Lett.* **76** 4046
Adams C P, Lynn J W, Mukovskii Y M, Arsenov A A and Shulyatev D A 2000 *Phys. Rev. Lett.* **85** 3954
[29] Bibes M, Balcells L, Fontcuberta J, Wojcik M, Nadolski S and Jedryka E 2003 *Appl. Phys. Lett.* **82** 928
[30] Zhang N, Ding W, Zhong W, Xing D and Du Y 1997 *Phys. Rev.* B **56** 8138
[31] Park J H, Vescovo E, Kim H-J, Kwon C, Ramesh R and Venkatesan T 1998 *Phys. Rev. Lett.* **81** 1953